Available online at www.sciencedirect.com
ScienceDirect
Solid State Ionics 178 (2007) 925–935
SOLID STATE IONICS
www.elsevier.com/locate/ssi

Characterization of sulfur poisoning of Ni–YSZ anodes for solid oxide fuel cells using *in situ* Raman microspectroscopy

Zhe Cheng, Meilin Liu *

School of Materials Science and Engineering, Georgia Institute of Technology, 771 Ferst Drive NW, Atlanta, GA 30332, United States

Received 7 November 2006; received in revised form 7 March 2007; accepted 5 April 2007

Abstract

The changes in the surface phase and the morphology of nickel–yttria stabilized zirconia (YSZ) cermet anodes for solid oxide fuel cells (SOFCs) upon exposure to a fuel containing 100 parts per million (ppm)-level hydrogen sulfide (H_2S) at elevated temperatures were investigated using *in situ* Raman microspectroscopy as well as *ex situ* techniques such as X-ray diffraction (XRD), scanning electron microscopy (SEM), and energy dispersive X-ray spectroscopy (EDX). The *in situ* Raman experiment revealed that nickel surfaces underwent significant sulfidation when the Ni–YSZ cermet was cooled slowly (at ~2–5 °C/min) from the testing temperature (~500–800 °C) to room temperature in a fuel with $pH_2S/pH_2 = 100$ ppm, although no sulfides were detected at elevated temperatures (>500 °C) in the same fuel. In comparison, the *ex situ* measurements at room temperature may not reflect what actually happens to samples during exposure to H_2S at elevated temperatures: results may be complicated by inevitable changes induced during the cooling of samples to room temperature in order to perform the *ex situ* measurements. Thus, *in situ* measurements are vital to the confirmation of the validity or even the relevance of the results from *ex situ* measurements in the study of the sulfur poisoning mechanism for Ni-based anodes of SOFCs.

Keywords: Solid oxide fuel cell (SOFC); Ni–YSZ cermet anode; Hydrogen sulfide (H_2S); *In situ* Raman spectroscopy

1. Introduction

The nickel–yttria stabilized zirconia (YSZ) cermet anode of a solid oxide fuel cell (SOFC) is readily poisoned by trace amounts of sulfur contaminants such as hydrogen sulfide (H_2S) in a fuel [1–10]. Previous studies indicate that the sulfur poisoning of an Ni–YSZ cermet anode is a two-stage process characterized by rapid cell performance degradation in the first few minutes (or up to several hours) followed by more gradual degradation that lasts for hundreds of hours or even longer; [1,6,8–10] the extent of sulfur poisoning strongly depends on cell operating temperature, H_2S concentration, cell voltage, and current density [1,5,8,10].

However, the mechanism for the sulfur poisoning of Ni-based anodes of SOFCs is still not clearly understood. Matsuzaki and Yasuda found that the critical H_2S concentration (above which the electrode activity started to degrade significantly) for an Ni–YSZ anode decreased from 2 parts per million (ppm) at 1000 °C to 0.05 ppm at 750 °C, and for a given H_2S concentration, the extent of performance degradation increased as the cell operating temperature decreased [5]. Based on these observations and the assumption that sulfur adsorbs more easily at lower temperatures, the authors suggested that sulfur poisoning is caused by the adsorption of sulfur on the electrode. Sasaki et al. analyzed the Ni–S–O phase diagram at 800 °C and concluded that anode poisoning by several ppm H_2S could not be explained by the formation of bulk nickel sulfide because bulk sulfide, for example, Ni_3S_2 (liquid phase), is stable only when the H_2S concentration is above ~2000 ppm at that temperature [6]. They claimed that though no obvious microstructural change was observed after the initial poisoning, agglomeration of Ni particles was observed after the failure of their cell. The authors attributed the initial poisoning to the dissociative adsorption of sulfur species around three-phase boundaries (TPBs) and the cell failure to the irreversible decrease in TPB length due to the agglomeration of Ni particles, which was

* Corresponding author. Tel.: +1 404 894 6114.
E-mail address: meilin.liu@mse.gatech.edu (M. Liu).

0167-2738/$ - see front matter © 2007 Elsevier B.V. All rights reserved.
doi:10.1016/j.ssi.2007.04.004

accelerated by the presence of sulfur. Xia and Birss, who found that only part of the sulfur poisoning was recoverable, hypothesized that the recoverable portion was due to the adsorption of sulfur or H_2S on active Ni-YSZ sites while the irrecoverable portion was due to the formation of a thin layer of nickel–sulfur compound such as Ni_3S_2 in the anode [7]. Waldbillig and colleagues claimed that nickel sulfide was not detected in sulfur-poisoned anodes using transmission electron microscopy (TEM) and scanning electron microscopy (SEM) coupled with energy dispersive X-ray spectroscopy (EDX); they concluded that after poisoning, Ni is covered by a monolayer of adsorbed sulfur instead of bulk nickel sulfide [8]. In contrast, using both X-ray photofluorescence spectroscopy (XPS) and EDX, Trembly et al. identified a significant amount of sulfur on the Ni-doped ceria cermet anode of an SOFC after running on a fuel containing 207 ppm H_2S at 850 °C for 650 h; the authors proposed that sulfur poisoning may be due to the formation of sulfur compounds such as NiS and/or CeS_2 [9].

To date, most previous studies on the sulfur poisoning of Ni–YSZ cermet anodes have been limited to the observation of the electrochemical response of an anode to sulfur content, *i.e.*, changes in cell current, voltage, or impedance spectra [1–5,7,10]. The actual chemical species on the anode surface and the accompanying microstructural changes of the Ni–YSZ cermet anode upon exposure to sulfur-containing fuels have not yet been systematically characterized, and no study has been carried out under an *in situ* condition (*i.e.*, at high temperature in fuels containing H_2S) [6,8,9]. Due to the lack of such studies, many discussion about the sulfur poisoning mechanism of the Ni–YSZ anode still remains partially speculative. On the other hand, the poisoning of metal catalysts such as nickel by trace amounts of sulfur has been studied for a long time. The structure of the sulfur overlayer on nickel, the bonding state, and the bonding energy at low temperatures (usually at or below room temperature) have been determined using conventional surface analysis techniques such as low energy electron diffraction (LEED), electron energy loss spectroscopy (EELS), Auger electron spectroscopy (AES), and XPS [11]. However, one limitation of these techniques is that they all require an environment of ultra-high vacuum: the sulfur–anode interaction may be different when the environment changes from a fuel atmosphere containing sulfur species to a vacuum.

Clearly, the most direct method of investigating the sulfur poisoning mechanism of an SOFC anode is to characterize the changes on the anode surface before and after exposure to a sulfur-contaminated fuel under an *in situ* condition, which can be accomplished using Raman spectroscopy. Previous studies have demonstrated that Raman has better sensitivity to a trace amount of nickel sulfide than conventional X-ray diffraction (XRD) [12–13], and *in situ* Raman has already been used to characterize catalysts or reaction species [14,15] and to monitor the reduction/oxidation cycle and the carbon formation for SOFC anodes [16]. In this study, *in situ* Raman microspectroscopy as well as *ex situ* characterization techniques such as conventional Raman, optical microscopy, XRD, SEM, and EDX were used to investigate the changes in the surface species and the microstructure of Ni–YSZ composites exposed to H_2S-containg fuels. The results were correlated with thermodynamic analysis to provide further insight into the mechanism for the sulfur poisoning of Ni-based anodes of SOFCs.

2. Experimental

2.1. Preparation of samples

The samples used in this study were dense composite pellets with 40 vol.% Ni and 60 vol.% YSZ. Ni powder (−300 mesh, Alfa Aesar) was first mixed with YSZ (containing 8 mol% Y_2O_3, 0.2–0.3 μm, Daiichi) for 1 h using a mortar and a pestle. The mixed powder was pressed into pellets in a 13-mm-diameter die at a pressure of 150 MPa. The pressed pellets were covered with Ni foils and sintered at 1375 °C for 5 h in 4% H_2/96% Ar with a heating and cooling rate of 5 °C/min. The sintered pellets were ground successively with SiC abrasive paper (P500, P800, and P1200, Struers) and polished with 1 μm α-alumina (Struers) suspension in water.

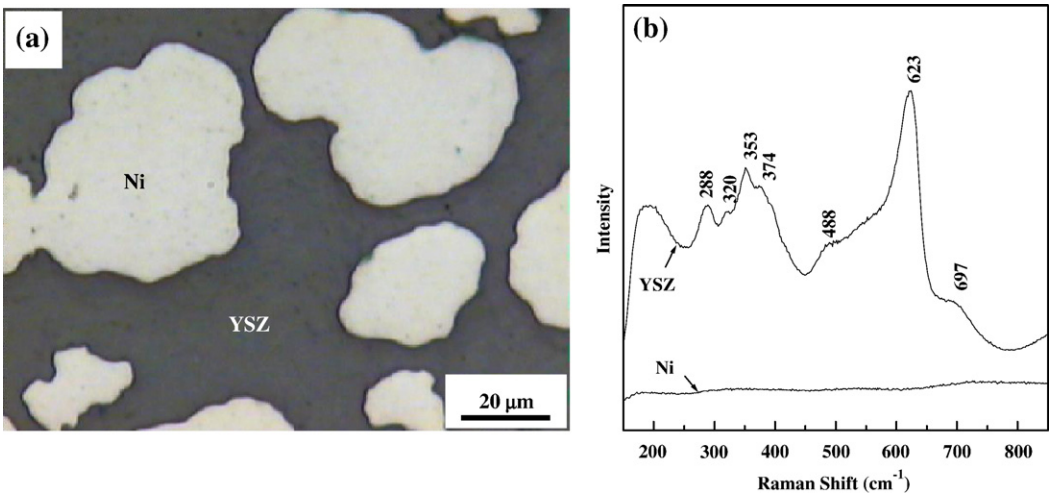

Fig. 1. (a) An optical microscopy image and (b) the corresponding Raman spectra from the YSZ and the Ni region on a polished surface of an as-prepared Ni–YSZ composite sample.

2.2. Ex situ characterizations

For *ex situ* experiments, the polished sample was put in an alumina boat, sealed in an alumina tube furnace, and heated up to a high temperature (*e.g.*, 800 °C) in a fuel with a nominal composition of 50 ppm H_2S/50% H_2/1.5% H_2O/48.5% N_2 by volume. After the sample was held at that temperature for a predetermined period of time, the sample was cooled down with the furnace in the same fuel. The time required for the furnace to cool from 800 °C to room temperature was ~5 h. After that, the sample was examined at room temperature using Raman microspectroscopy (Renishaw 2000, 514 nm laser, 40 mW), XRD (PW1800 X-ray diffractometor, Philips Analytical, Cu-Kα line), SEM (S800, Hitachi, 10 kV), and EDX (3600-0398, Kevex X-ray).

2.3. In situ characterizations

The *in situ* Raman experiment was carried out in a Raman cell with a quartz window (HVC-DRP-1, Harrick Scientific). An Ni–YSZ composite pellet with a polished surface was mounted onto the sample stage of the Raman cell using a gold paste (C5755A, Heraeus), which was then cured by heating up the Raman cell in open air to ~250 °C (the sample temperature was calibrated using a type-K thermal couple connected to an Omega HH506R digital thermometer as well as high purity metal melt standards such as tin (T_m=232 °C, TA Instruments) and zinc (T_m=420 °C, TA instruments).) Then the Raman cell was sealed with a quartz window and purged with nitrogen. After that, the nitrogen gas was replaced by a sulfur-free fuel (usually 50% H_2/1.5% H_2O/48.5% N_2), and the cell was heated up to the measuring temperature (*e.g.*, ~570 °C). At that temperature, Raman spectra as well as optical images showing surface morphology were recorded before and after a trace amount of H_2S (pH_2S/pH_2=100 ppm) was introduced into the Raman cell. In addition, the Raman cell was also cooled at different rates in a fuel with or without H_2S to monitor the changes in the surface species and the morphology of the sample.

3. Results

3.1. Characterization of the as-prepared Ni–YSZ composite sample

Fig. 1(a) shows an optical micrograph of the polished surface of a dense Ni–YSZ composite. The bright, often isolated

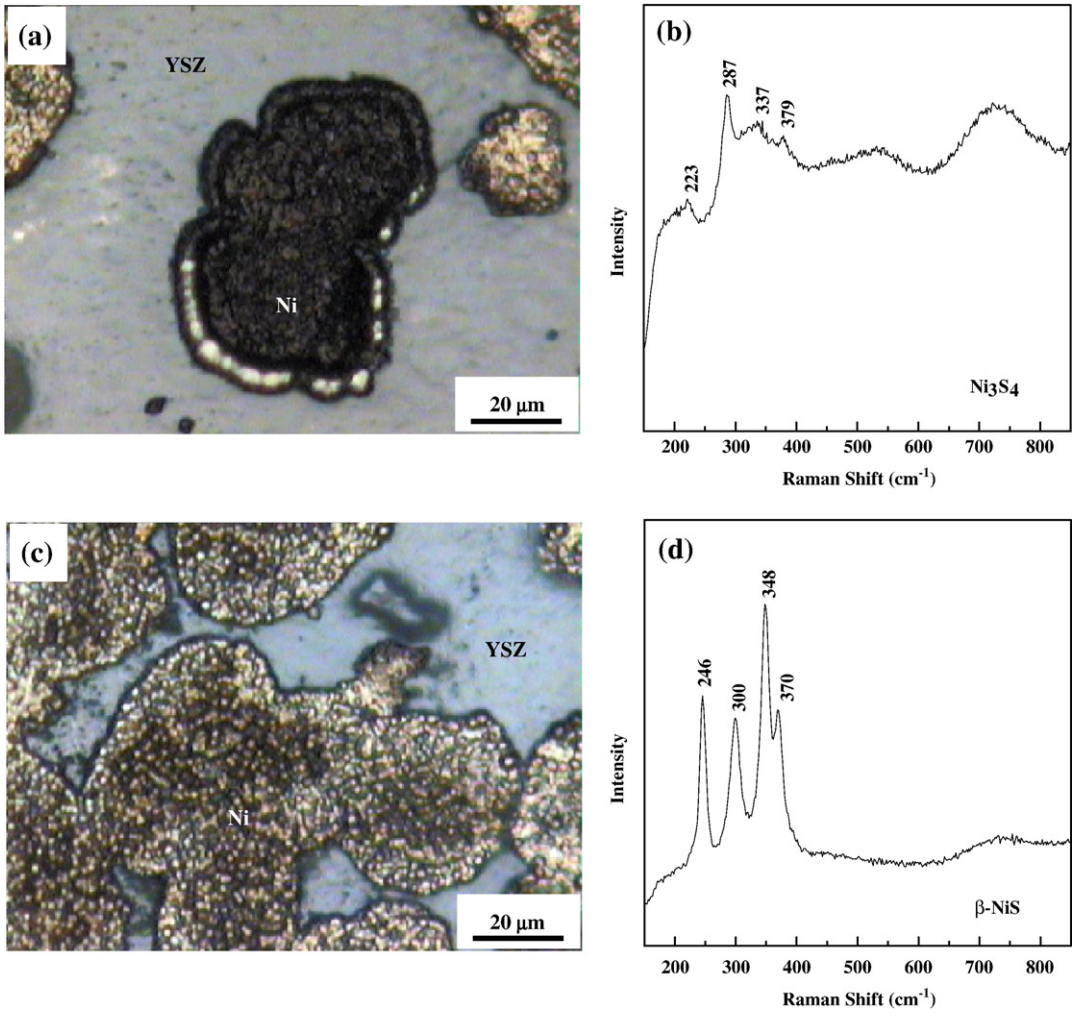

Fig. 2. Optical microscopy images (a, c) and the corresponding Raman spectra (b, d) taken from the Ni region of the Ni–YSZ composite after exposure to an H_2S-containing fuel (50 ppm H_2S/50% H_2/1.5% H_2O/48.5% N_2) at 800 °C for 2 h 45 min.

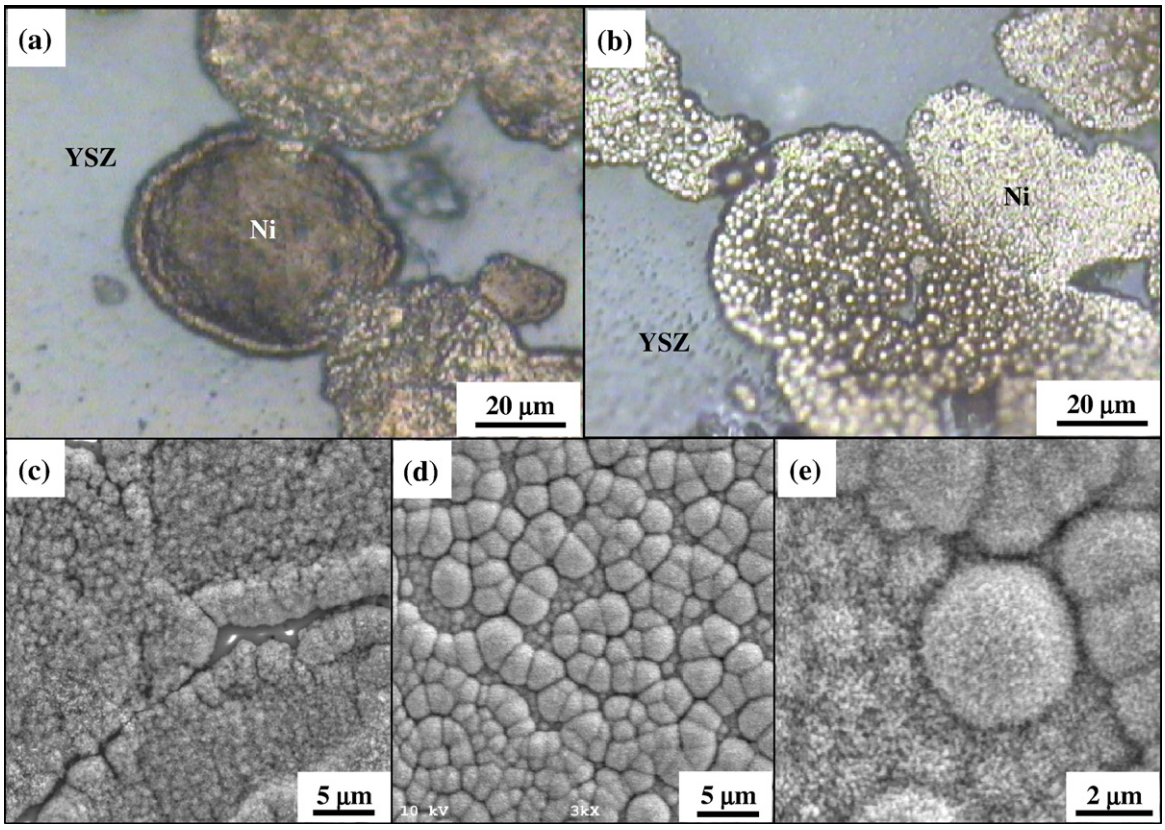

Fig. 3. Optical microscopy (a, b) and SEM (c, d, e) images of the Ni–YSZ composite after exposure to an H_2S-containing fuel (50 ppm H_2S/1.5% H_2O/48.5% N_2/50% H_2) at 800 °C for 48 h.

regions are Ni, and the gray regions are YSZ. Fig. 1(b) shows the typical Raman spectra taken from the Ni and the YSZ regions. While the Raman spectrum for the Ni region is essentially featureless, the Raman spectrum for the YSZ region has one strong band at ~623 cm^{-1} and several weaker bands or shoulders at 288, 320, 353, 374, 488, and 697 cm^{-1}. The appearance of multiple bands for the YSZ phase indicates that the surface of the YSZ is not a perfect cubic structure but has tetragonal or monoclinic distortions [17–20]. The Ni–YSZ composite was used to mimic the conventional porous Ni–YSZ cermet anode for an SOFC. Compared with the cermet anode with micron-scale Ni and YSZ grains, which are very difficult to distinguish under an optical microscope or an SEM, the dense composite sample with large sizes of Ni and YSZ grains allows easy characterizations of the individual Ni and YSZ phases as well as the boundaries between them using spatially-resolving techniques such as Raman microspectroscopy, SEM, and EDX elemental mapping. The problem of signals from different phases (*e.g.*, nickel sulfide and YSZ) overlapping one another would also be minimized compared with the conventional porous Ni–YSZ

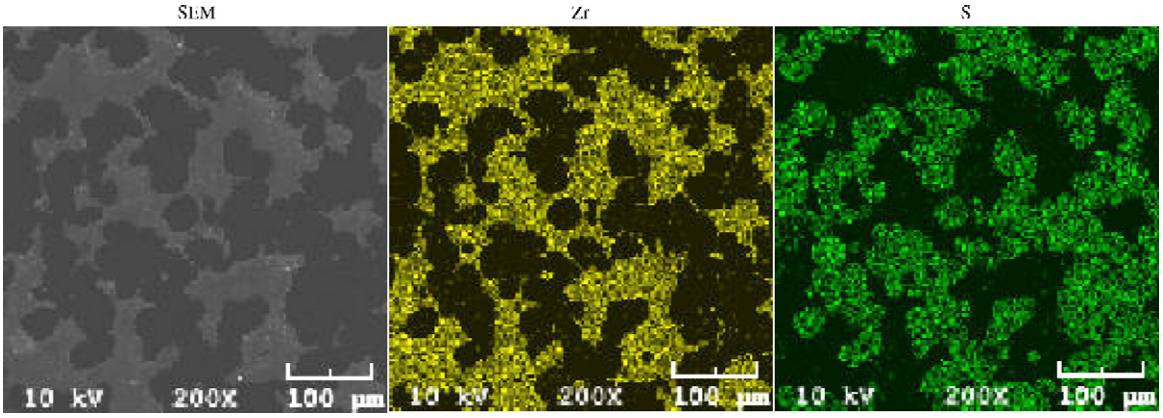

Fig. 4. SEM image and EDX elemental maps of the Ni–YSZ composite after exposure to an H_2S-containing fuel (50 ppm H_2S/1.5% H_2O/48.5% N_2/50% H_2) at 800 °C for 48 h (the full length of the scale bar is 100 μm.).

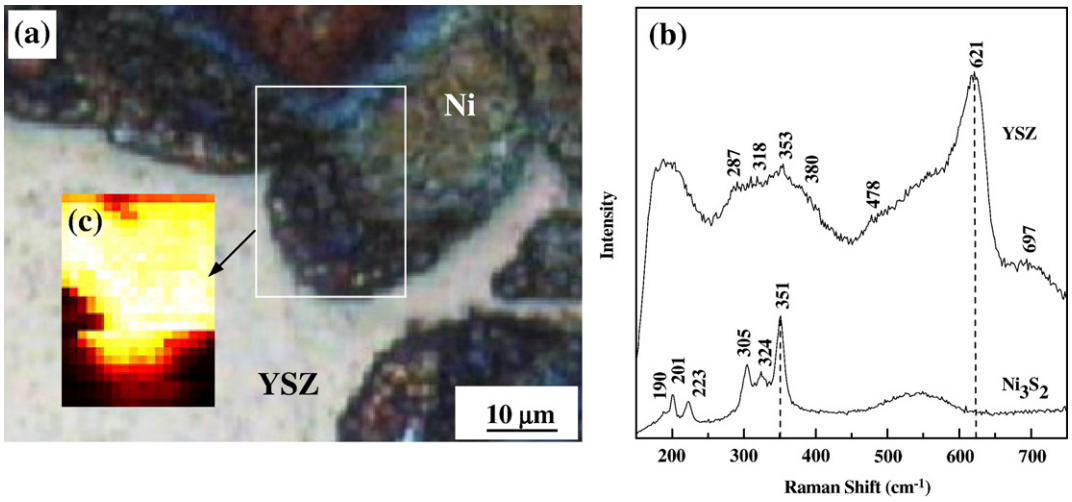

Fig. 5. Optical microscopy image (a), typical Raman spectra taken from the Ni and YSZ regions (b), and the corresponding Raman map for the circled region (c) of the Ni–YSZ composite after exposure to 50 ppm H_2S/1.5% H_2O/48.5% N_2/50% H_2 at 800 °C for 18 h followed by annealing at 500 °C for 2 h in 4% H_2/3% H_2O/93% Ar.

cermet, for which the signal (*e.g.*, Raman) from the YSZ grains is often overwhelmingly strong, burying changes in the spectra from the Ni grains.

3.2. Ex situ characterizations of the Ni–YSZ composite after exposure to H_2S-containing fuel

The research on changes that take place on the Ni–YSZ composite surface after exposure to H_2S started with *ex situ* experiments. Fig. 2 shows optical microscopy images and the corresponding Raman spectra taken from a sample after it was exposed to a fuel mixture of 50 ppm H_2S/50% H_2/1.5% H_2O/48.5% N_2 at 800 °C for 2 h 45 min and then cooled down gradually in the furnace while being exposed to the same fuel. The sample surface morphology has changed significantly. Some areas of the Ni particles appear darker, and the edge of the Ni particles rises above the center and the surrounding YSZ, as shown in Fig. 2(a). The Raman spectrum taken from the dark region on the Ni grain shows a sharp band at 287 cm^{-1} and three smaller bands at 223, 337, and 379 cm^{-1} (Fig. 2(b)), all of which correspond to Ni_3S_4 [21,22]. In some other regions, the surface of Ni is full of sphere-like structures with diameters of ~1–3 μm, as shown in Fig. 2(c). Raman bands at 246, 300, 348, and 370 cm^{-1}, which closely match those of β-NiS [22–26], were obtained from those regions (Fig. 2(d)). Meanwhile, no observable changes in the surface morphology or the Raman signal were detected from the YSZ region. The continued exposure of the Ni–YSZ composite to the same fuel (50 ppm H_2S/50% H_2/1.5% H_2O/48.5% N_2) for a longer period of time (up to 48 h) at 800 °C did not lead to further observable changes in either the surface morphology or the Raman spectra from the Ni regions (Fig. 3(a) and (b)).

Closer examination using SEM confirms the drastic change in surface morphology on the Ni surface. Fig. 3 shows the optical and SEM micrographs of the Ni–YSZ composite exposed to a fuel mixture of 50 ppm H_2S/50% H_2/1.5% H_2O/48.5% N_2 for 48 h. Similar to the sample exposed to 50 ppm H_2S for 2 h 45 min, in some regions, the edge of the Ni particles rises above Ni and YSZ (Fig. 3(a) and (c)) and in other regions, the Ni surface is covered by micron-scale, sphere-like structures (Fig. 3(b), (d), and (e)). The SEM images show that the surfaces of the spheres and the regions in between are composed of submicron-scale, irregular-shaped particles (Fig. 3(d) and (e)).

The distribution of sulfur on a sample was characterized by EDX elemental mapping. Fig. 4 shows the low magnification SEM image and the corresponding Zr- and S-elemental maps of the Ni–YSZ composite exposed to 50 ppm H_2S/50% H_2/1.5% H_2O/48.5% N_2 at 800 °C for 48 h. The distribution of sulfur and zirconium complement one another, indicating that sulfur selectively attacks nickel in the composite. The fact that sulfur was not detectable in the YSZ region is consistent with the observation that the Raman signal from the YSZ region did not change much after the H_2S exposure; it is also reasonable since YSZ does not react with H_2S or sulfur and the adsorption of sulfur on oxides is usually minimal (see Ref. [11], p. 157).

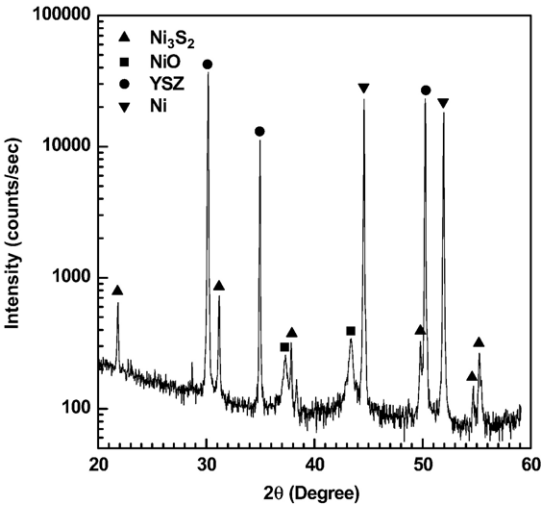

Fig. 6. XRD pattern of the Ni–YSZ composite after exposure to 50 ppm H_2S/1.5% H_2O/48.5% N_2/50% H_2 at 800 °C for 18 h followed by annealing at 500 °C for 2 h in 4% H_2/3% H_2O/93% Ar.

While EDX identifies where sulfur is on the dense Ni–YSZ composite, it is unable to determine what the sulfur-containing phases are. Its sensitivity to surface species is also limited due to the large sampling volume. In contrast, the identification and the mapping of the sulfur-containing phase on the Ni–YSZ composite surface could be achieved simultaneously using the Raman mapping technique with a spatial resolution of ~1 μm [14]. Fig. 5 shows the optical microscopy image, typical Raman spectra, and the corresponding Raman map taken from a 25 × 18 μm area (enclosed by the rectangular outline) in a sample exposed to 50 ppm H_2S/1.5% H_2O/48.5% N_2/50% H_2 at 800 °C for 18 h followed by annealing at 500 °C for 2 h in 4% H_2/3%

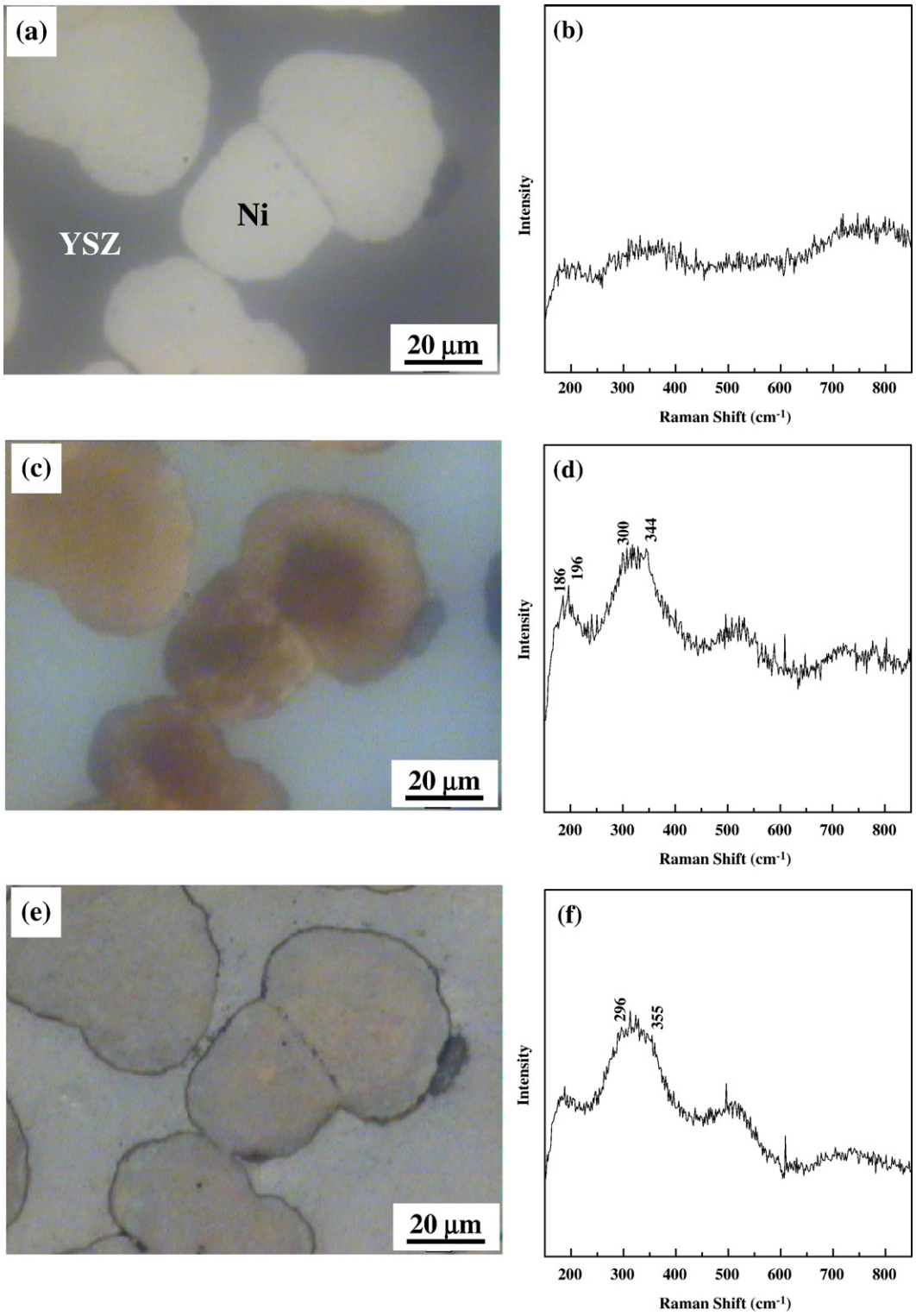

Fig. 7. Optical microscopy images (a, c, e) and corresponding *in situ* Raman spectra (b, d, f) taken from the Ni region for a Ni–YSZ composite when exposed to an H_2S-containing fuel (50 ppm H_2S/1.5% H_2O/48.5% N_2/50% H_2) at 500 °C (a, b), and cooled at 2.5 °C/min to 216 °C (c, d) and 20 °C (e, f) successively.

H_2O/93% Ar. Basically, Raman spectra were obtained point-by-point from the region with a step size of 1 μm. The typical Raman spectra obtained from the Ni region (darker) and the YSZ region (brighter) are shown in Fig. 5(b). The spectrum from the Ni region corresponds to Ni_3S_2 (Heazlewoodite phase) [22,26], which is also confirmed using XRD, as shown in Fig. 6 (previous references [12,13,24] are not correct about the Raman spectrum for Ni_3S_2 [22,26]). NiO, as indicated in the XRD pattern, must come from the slight oxidation of nickel sulfide at lower temperatures due to exposure to the air, and NiO does not have sharp Raman features below the wave number of 350 cm^{-1}. The examination of all the spectra obtained shows that the Ni surface was uniformly covered by Ni_3S_2. Since the Raman signal for YSZ is stronger than that for Ni_3S_2, the Raman map (Fig. 5(c)) was obtained by plotting the ratio of the signal at 351 cm^{-1} to that at 621 cm^{-1} with respect to the position on the sample surface. A large ratio (the brighter part in the map) indicates Ni_3S_2, a small ratio (the darker part in the map) indicates YSZ, and an intermediate ratio indicates both phases (close to the boundary between the Ni and the YSZ phases). Compared with XRD (Fig. 6) that shows a majority of Ni and YSZ with a trace amount of Ni_3S_2, Raman mapping is more sensitive to the phase on the surface (in fact, Raman is active to nickel sulfide film with thickness as small as ~10 nm while the conventional XRD cannot detect the sulfide phase [27]). It also characterizes sulfide distribution with a spatial resolution of ~1 μm, which is unattainable by conventional XRD.

3.3. *In situ* characterization of the Ni–YSZ composite during exposure to H_2S-containing fuel using Raman microspectroscopy

Based on the results of the *ex situ* experiments, it looks as if various bulk nickel sulfides (*i.e.*, Ni_3S_4, β-NiS, and Ni_3S_2) form on the surface of nickel and inflict dramatic morphology change when the Ni–YSZ composite is exposed to an H_2S-containing fuel at elevated temperatures. To investigate whether this is the reason for the sulfur poisoning of the Ni-based anode for an SOFC, *in situ* Raman microspectroscopy was carried out to determine when various sulfides form and surface morphology changes. The focus of the study was on the Ni region because no significant change had been identified on the YSZ region by the *ex situ* experiments.

Fig. 7(a) and (b) shows the optical image and the corresponding Raman spectra taken from the Ni region for an Ni–YSZ composite at ~500 °C in a fuel of 50 ppm H_2S/1.5% H_2O/48.5% N_2/50% H_2 after it had been exposed to the same fuel at ~570 °C for 5 h. No significant changes in either morphology or Raman signal were observed on the Ni surface. However, when that sample was cooled down at a rate of 2.5 °C/min, the surface of Ni started to change gradually as the sample temperature dropped below ~350 °C. Fig. 7(c) and (d) shows the optical image and the corresponding Raman spectrum taken from the same region after the sample was cooled at 2.5 °C/min to 216 °C and held at 216 °C for 0.5 h. Accompanying brown regions that appeared on the Ni surface was a Raman spectrum that showed peaks at 186 and 196 cm^{-1} and a broad band in the range of ~300–344 cm^{-1}, most likely corresponding to Ni_3S_2 [22,26]. Continued exposure to the same fuel (pH_2S/pH_2=100 ppm) at 216 °C and below led to further changes in surface morphology and the Raman spectrum (see Fig. 7(e) and (f)), indicating that the sulfidation reaction was probably producing nickel sulfide phases with an even higher sulfur content (*e.g.*, Ni_7S_6).

In comparison, when a post-exposure sample was cooled down quickly at a rate of ~70 °C/min to room temperature in the same H_2S-contaminated fuel, no observable changes in either surface morphology or the Raman spectrum could be identified, as shown in Fig. 8, which suggests that nickel sulfides form slowly in an intermediate temperature range (~100 to 400 °C), and if the total exposure time in that temperature range is short (*i.e.*, within a few minutes), the amount of sulfide formed would be negligible.

To investigate whether the sulfide formed at intermediate temperatures (*e.g.*, 216 °C) will remain when heated to an

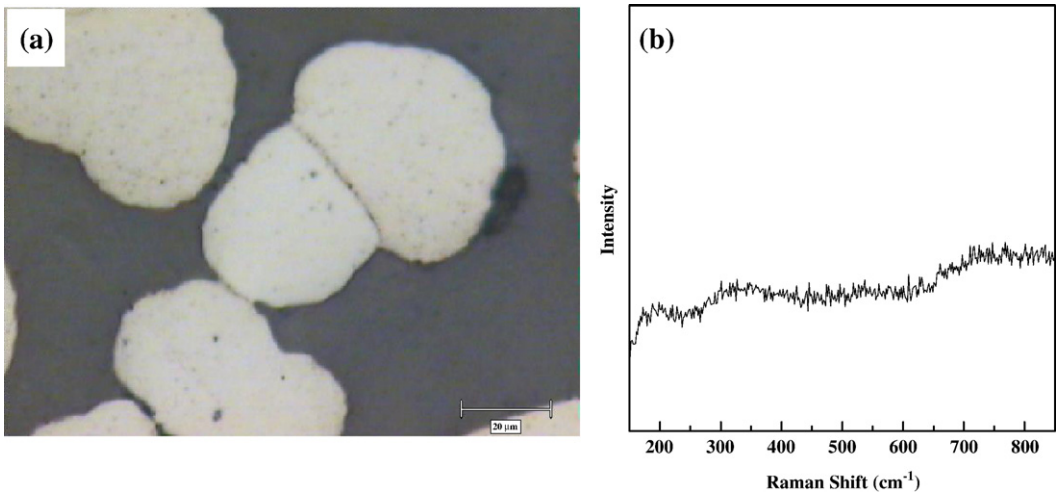

Fig. 8. Optical microscopy image (a) and the corresponding *in situ* Raman spectrum (b) taken from the Ni region for a Ni–YSZ composite after it was exposed to an H_2S-containing fuel (50 ppm H_2S/1.5% H_2O/48.5% N_2/50% H_2) at 570 °C for 5 h and cooled to room temperature at ~70 °C/min.

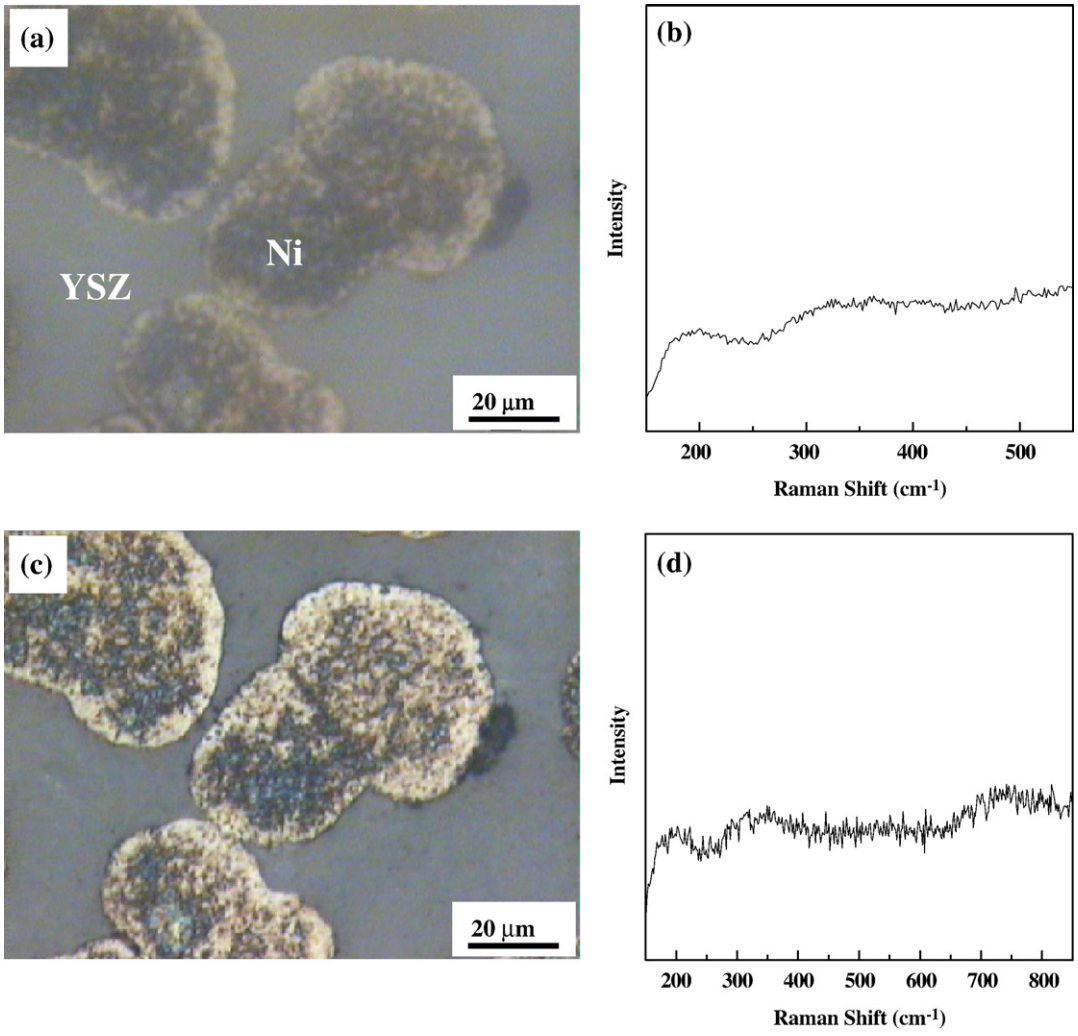

Fig. 9. Optical microscopy images (a, c) and the corresponding *in situ* Raman spectra (b, d) taken from the Ni region for a Ni–YSZ composite after exposure to H_2S-containing fuel (50 ppm H_2S/1.5% H_2O/48.5% N_2/50% H_2) at 570 °C, followed by cooling at 2.5 °C/min to room temperature, reheating to ≥500 °C (a, b) and cooling again at ~70 °C/min to room temperature (c, d).

elevated temperature, the same sample (see the description for Fig. 7) was reheated in the fuel with $pH_2S/pH_2 = 100$ ppm inside the Raman cell after it was cooled down to room temperature at 2.5 °C/min. During the reheating process, the surface morphology changed and the Raman bands corresponding to nickel sulfides disappeared gradually. At ~500 °C, the surface of the Ni grain became non-uniform and the Raman spectrum was the same as that for pure Ni (Fig. 9(a) and (b)). After being heated up to ~570 °C and held for another 12 h, the sample was cooled down in the same fuel at ~70 °C/min again. This time, the morphology did not change further (Fig. 9(c)) and no Raman band corresponding to sulfides could be identified (Fig. 9(d)), which is consistent with the result shown in Fig. 8.

4. Discussion

Contrary to the results of the *ex situ* experiments shown first, the results of the *in situ* Raman experiment suggest that (i) no conventional nickel sulfide (*e.g.*, Ni_3S_2 and NiS) formed on the Ni–YSZ composite surface at high temperatures (>~500 °C) in a fuel with $pH_2S/pH_2 = 10^{-4}$ (or 100 ppm), and (ii) the nickel sulfides observed in the *ex situ* experiments (Ni_3S_4, β-NiS, and Ni_3S_2) must have accumulated during the slow cooling process in the furnace due to the reaction between H_2S and Ni, which also caused the dramatic morphology change. Such an argument is supported by the fact that slow cooling (*e.g.*, ~2–5 °C/min) or low temperature exposure (*e.g.*, at 216 °C) of the Ni–YSZ composite in the H_2S-containing fuel led to the formation of significant amounts of various nickel sulfides and dramatic changes in surface morphology (Figs. 2–4 and 7(c)–(f)) whereas fast cooling (70 °C/min) from ~570 °C to 20 °C in the same fuel did not lead to detectable changes in Raman spectra (Figs. 8 and 9(c)–(d)).

The above argument is also supported by the EDX characterization of the Ni–YSZ composite sample cooled at different rates in the H_2S-containing fuel. Fig. 10 shows the SEM image, the Zr element map, and the EDX spectrum taken from the Ni region for the Ni–YSZ composite sample after the *in situ* experiment and cooled quickly at ~70 °C/min in a fuel with $pH_2S/pH_2 = 10^{-4}$ (see the description for Figs. 7 and 9).

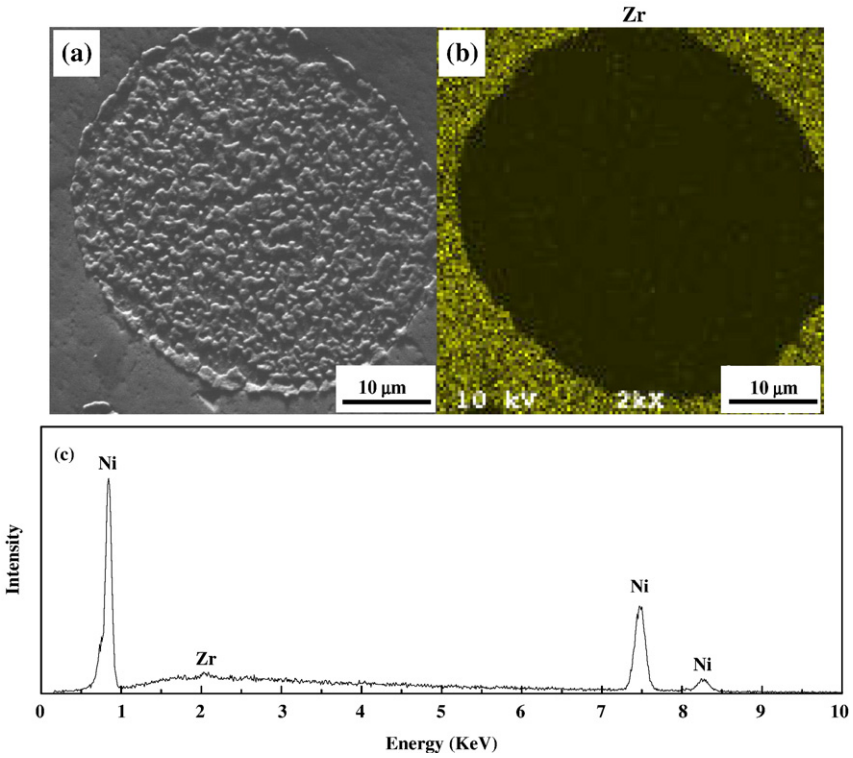

Fig. 10. (a) A SEM image, (b) the corresponding Zr elemental map, and (c) the EDX spectrum from the Ni region of a Ni–YSZ composite after exposure to H_2S-containing fuel (50 ppm H_2S/1.5% H_2O/48.5% N_2/50% H_2) at 570 °C, followed by cooling at 2.5 °C/min to room temperature, reheating to ≥500 °C (a, b) and cooling again at ~70 °C/min to room temperature.

No sulfur was identified from the Ni region. By comparison, significant amount of sulfur is present on the nickel surface when the sample was cooled slowly with the furnace, as shown in Fig. 4. A third piece of evidence for the argument is that no observable changes in morphology, the Raman signal, or the EDX spectrum could be identified when the Ni–YSZ composite was cooled (quickly or slowly) in an H_2S-free fuel after it was exposed to an H_2S-containing fuel at an elevated temperature.

The observation of conventional nickel sulfide formation on the Ni surface at intermediate temperature (~100–400 °C) is not unexpected from a thermodynamics point of view. Although bulk nickel sulfides are not stable at 800 °C in a fuel with $p\mathrm{H_2S}/p\mathrm{H_2}=100$ ppm, the equilibrium $p\mathrm{H_2S}/p\mathrm{H_2}$ ratio decreases dramatically as the temperature drops from 800 °C to a lower temperature. In fact, according to the Ni–S phase diagram constructed by Rosenqvist [28], Ni_3S_2 becomes thermodynamically stable at temperatures below ~420 °C when $p\mathrm{H_2S}/p\mathrm{H_2}=10^{-4}$. Based on the thermodynamic analysis using the data in a standard reference [29], even the more sulfur-rich β-NiS and Ni_3S_4 phases will also become thermodynamically stable at a temperature below ~250 and ~160 °C, respectively, when $p\mathrm{H_2S}/p\mathrm{H_2}=10^{-4}$, which could explain the appearance of β-NiS and Ni_3S_4 in the *ex situ* experiments (Fig. 2). The observation of various sulfides on Ni surfaces is also consistent with those of previous investigations showing that the corrosion of Ni starts with the formation of Ni_3S_2, and the outer layer of the sulfide scale consists of more sulfur-rich phases such as Ni_7S_6 and then β-NiS [30].

The dramatic morphologies such as balls and ridges observed on Ni surfaces (Figs. 2 and 3) are most likely due to the swelling effect of the sulfidation of Ni: the volume expansion from Ni to Ni_3S_2 and from Ni to β-NiS (as calculated from the information in JCPDS card) is 107% and 150%, respectively. The dramatic morphologies may also be related to the decrease in the melting point for nickel sulfide (*e.g.*, Ni_3S_2) with the decrease in the $p\mathrm{H_2S}/p\mathrm{H_2}$ ratio as indicated by the Ni–S phase diagram [28]. The morphology change caused by nickel sulfide formation is not reversible after the sulfide decomposes back to Ni, as evidenced by the scarred Ni surface shown in Fig. 10, which indicates that commercial SOFCs should not be cooled in fuels containing hundreds of ppm H_2S to avoid irreversible microstructural changes.

The comparison of the *in situ* Raman microscopy with other *ex situ* experiments clearly illustrates the importance and the effectiveness of the *in situ* technique, which provides combined information about the identity, the microstructure, and the distribution of phases on the anode surface at elevated temperatures in an atmosphere close to the fuel cell operating condition. In contrast, all other conventional surface analysis methods such as XPS, AES, LEED, and EELS require a certain level of a vacuum. While some of them offer much higher sensitivity and/or spatial resolution, the sample preparation for *ex situ* measurements should only be carried out with great care since many experimental parameters may influence the observed results and their interpretations. The key challenge is to preserve the sample (especially the surface composition and

structure) as it is cooled from the testing temperature to room temperature and transferred from a fuel environment to a vacuum. As stated, the thermodynamic driving force for H_2S to react with nickel and form bulk nickel sulfide increases as the temperature decreases. Therefore, if a sample exposed to ppm-level H_2S at a high temperature (*e.g.*, 800 °C) is cooled in an H_2S-containing fuel, bulk sulfide may form at intermediate temperatures (*e.g.*, ~200–400 °C); on the other hand, if the sample is cooled in a fuel without H_2S, some adsorbed sulfur atoms on the surface may be removed by hydrogen to form H_2S. The possible solution is to cool the sample quickly enough in a clean environment to preserve the surface. However, which media and how the dramatic temperature change influences the distribution of sulfur on the surface should be considered before the experiment.

The formation of conventional nickel sulfide (*e.g.*, Ni_3S_2) on the nickel surface is unlikely to be responsible for the observed degradation in anode performance (or Ni poisoning) because (i) thermodynamic analysis indicates that conventional nickel sulfides are not stable under the typical SOFC testing condition [6,28,31], and (ii) no conventional nickel sulfide was detected on the surface of the Ni–YSZ composite using *in situ* Raman spectroscopy at elevated temperatures (*i.e.*, >500 °C) in fuels with $pH_2S/pH_2 = 100$ ppm. However, sulfur does adsorb on the surface of Ni under the conditions for fuel cell operation, as predicted by density function theory (DFT) calculations [32] and as determined in other studies [11]. The authors believe that the sulfur adsorption on the nickel surface is responsible for the first stage of sulfur poisoning for the Ni–YSZ anode (as characterized by a sharp performance drop) due to the quick speed of the poisoning process (sometimes within a few minutes) and the low concentration (down to 0.05 ppm at 750 °C) required to poison the anode [1,5,6,8–10]. The mechanism for the second stage of sulfur poisoning, characterized by a slower but continuous performance drop that lasts for hundreds of hours, is still not clear [10], but it may be one of the following possible explanations: (i) the adsorbed sulfur atoms penetrate into the Ni grains following bulk phase diffusion kinetics, which may change the surface structure and electrical and electrochemical performance of the Ni-based anode; (ii) sulfur may be adsorbed on the nickel surface that is more difficult to access (such as in a pore with a narrow opening); (iii) the adsorbed sulfur might incur surface reconstruction of the Ni, for example from (111) surface to (100) surface (see the review by Bartholomew [11], p. 143), and the reaction kinetics may vary according to the different Ni crystallography planes; and (iv) the interaction of sulfur with the electrolyte may also influence the behavior of the anode. Determining which of these mechanisms is responsible for the second-stage poisoning requires further experiments. For example, the first may be studied by a depth profile analysis of the sulfur element after different time of exposure of a dense Ni–YSZ composite to an H_2S-contaminated fuel; the second may be tested by long-term poisoning experiments to see if sulfur poisoning will saturate; the third may be tested by the time requested for the surface to reconstruct; and the last could be investigated using different electrolyte components, which determines the influence of electrolytes on the sulfur poisoning behavior. In addition, more sensitive Raman measurements such as surface enhanced Raman spectroscopy (SERS) and tip-enhanced Raman spectroscopy (TERS), combined with other surface analysis techniques, may also provide further insight into the sulfur poisoning mechanism of SOFC anodes.

5. Conclusions

Various bulk nickel sulfides and dramatic morphology changes were observed on the Ni surfaces of a Ni–YSZ composites after the exposure to fuels with $pH_2S/pH_2 = 100$ ppm at elevated temperatures using *in situ* Raman microspectroscopy and several *ex situ* characterization techniques. The *in situ* Raman study indicates that sulfur poisoning of a Ni–YSZ anode is not due to the formation of conventional nickel sulfides; the formation of the sulfide and the changes in morphology observed in the *ex situ* experiments actually occurred during the slow cooling process as a result of the reactions between bulk Ni and H_2S. A comparison of the results from *in situ* Raman with those from the *ex situ* techniques illustrates the importance and effectiveness of the *in situ* method in the study of the sulfur poisoning mechanism for Ni-based anodes of SOFCs. *Ex situ* experiments should be carried out with great caution to prevent any artifacts induced by sample preparation. Further studies on the behavior of long-term sulfur poisoning the depth profile of sulfur within the Ni–YSZ composite, and the interaction of sulfur with the electrolyte are required to completely reveal the sulfur poisoning mechanism of the SOFC anode.

Acknowledgements

This work was supported by the DOE–NETL SECA Core Technology Program under award number DE-FC26-04NT42219. The authors would like to thank Dr. Shaowu Zha and Mr. Harry Abernathy for their help with some of the experiments and their valuable contributions to discussion.

References

[1] S.C. Singhal, R.J. Ruka, J.E. Bauerle, C.J. Spengler, Anode Development for Solid Oxide Fuel Cells, Final Technical Report, DOE/MC/22046-2371 (NIST Order No. DE87011136), U. S. Department of Energy, Washington, DC, 1986.
[2] D.W. Dees, U. Balachandran, S.E. Dorris, J.J. Heiberger, C.C. McPheeters, J.J. Picciolo, Proceedings of the First International Symposium on Solid Oxide Fuel Cells, The Electrochemical Society Proceedings Series, vol. 89–11, The Electrochemical Society, Pennington, NJ, 1989, p. 317.
[3] J. Geyer, H. Kohlmüller, H. Landes, R. Stübner, Proceedings of the Fifth International Symposium on Solid Oxide Fuel Cells, The Electrochemical Society Proceedings Series, vol. 97–40, The Electrochemical Society, Pennington, NJ, 1997, p. 585.
[4] S. Primdahl, M. Mogensen, Proceedings of the Sixth International Symposium on Solid Oxide Fuel Cells, The Electrochemical Society Proceedings Series, vol. 99–19, The Electrochemical Society, Pennington, NJ, 1999, p. 530.
[5] Y. Matsuzaki, I. Yasuda, Solid State Ionics 132 (2000) 261.
[6] K. Sasaki, K. Susuki, A. Iyoshi, M. Uchimura, N. Imamura, H. Kusaba, Y. Teraoka, H. Fuchino, K. Tsujimoto, Y. Uchida, N. Jingo, Proceedings of

the Ninth International Symposium on Solid Oxide Fuel Cells, The Electrochemical Society Proceedings Series, vol. 2005–07, The Electrochemical Society, Pennington, NJ, 2005, p. 1267.
[7] S.J. Xia, V.I. Birss, Proceedings of the Ninth International Symposium on Solid Oxide Fuel Cells, The Electrochemical Society Proceedings Series, vol. 2005–07, The Electrochemical Society, Pennington, NJ, 2005, p. 1275.
[8] D. Waldbillig, D.G. Ivey, A. Wood, Proceedings of the First International Symposium on Fuel Cell and Hydrogen Technologies, Canadian Institute of Mining, Metallurgy and Petroleum, Montreal, Canada, 2005, p. 237.
[9] J.P. Trembly, A.I. Marquez, T.R. Ohrn, D.J. Bayless, J. Power Sources 158 (2006) 263.
[10] S. Zha, Z. Cheng, M. Liu, J. Electrochem. Soc. 154 (2007) B201.
[11] C.H. Bartholomew, P.K. Agrawal, J.R. Katzer, Advances in Catalysis 31 (1982) 135.
[12] J. Dong, S. Zha, M. Liu, Proceedings of the Ninth International Symposium on Solid Oxide Fuel Cells, The Electrochemical Society Proceedings Series, vol. 2005–07, The Electrochemical Society, Pennington, NJ, 2005, p. 1284.
[13] J. Dong, Z. Cheng, S. Zha, M. Liu, Journal of Power Sources 156 (2006) 461.
[14] E. Smith, G. Dent, Modern Raman Spectroscopy— A Practical Approach, John Wiley & Sons, England, 2005.
[15] J.M. Stencel, Raman Spectroscopy for Catalysis, Van Nostrand Reinhold, New York, 1990.
[16] M.B. Pomfret, J.C. Owrutsky, R.A. Walker, Journal of Physical Chemistry B 110 (2006) 17305.
[17] C. Li, M. Li, Journal of Raman Spectroscopy 33 (2002) 301.
[18] D.W. Liu, C.H. Perry, R.P. Ingel, Journal of Applied Physics 64 (1988) 1413.
[19] J. Moon, H. Choi, Y. Kim, C. Lee, Journal of Materials Science Letters 20 (2001) 1611.
[20] A. Sekulic, K. Furic, A. Tonejc, A.M. Tonejc, M. Stubicar, Journal of Materials Science Letters 16 (1997) 260.
[21] RRUFF database of Raman dpectra, X-ray Diffraction and Chemistry Data for Minerals, The University of Arizona, http://rruff.info/index.php.
[22] J. Wang, Z. Cheng, M. Liu, in preparation.
[23] D.W. Bishop, P.S. Thomas, A.S. Ray, Materials Research Bulletin 33 (1998) 1303.
[24] D.W. Bishop, P.S. Thomas, A.S. Ray, Materials Research Bulletin 35 (2000) 1123.
[25] G. Shen, D. Chen, K. Tang, C. An, Q. Yang, Y. Qian, Journal of Solid State Chemistry 173 (2003) 227.
[26] Z. Cheng, M. Liu, in preparation.
[27] Z. Cheng, S. Choi, M. Liu, in preparation.
[28] T. Rosenqvist, Journal of the Iron and Steel Institute 176 (1954) 37.
[29] M.W. Chase Jr., C.A. Davies, J.R. Downey Jr., D.J. Frurip, R.A. McDonald, A.N. Syverud, JANAF Thermochemical Tables, Third editionAmerican Chemical Society, Washington DC, 1985.
[30] B.D. Bastow, G.C. Wood, Oxidation of Metals 9 (1975) 473.
[31] Z. Cheng, S. Zha, M. Liu, Journal of the Electrochemical Society 153 (2006) A1302.
[32] J.-H. Wang, M. Liu, in preparation.